

Focal Plane CCD Camera for the X-Ray Telescope (XRT) aboard SOLAR-B

Taro Sakao^{*a}, Ryouhei Kano^b, Hirohisa Hara^b, Keiichi Matsuzaki^a, Masumi Shimojo^b, Saku Tsuneta^b, Takeo Kosugi^a, Kiyoto Shibasaki^b, Kazuyoshi Kumagai^b, Masaki Sawa^b, Tomonori Tamura^b, Satoru Iwamura^c, Mitsuhiro Nakano^c, Zhangong Du^c, Kenji Hiyoshi^d, Michihiro Horii^d, Leon Golub^e, Jay A. Bookbinder^e, Peter C. Cheimets^e, Lawrence D. Hill^f, Jerry K. Owens^f

^aInstitute of Space and Astronautical Science, Japan Aerospace Exploration Agency, 3-1-1 Yoshinodai, Sagamihara, Kanagawa 229-8510, Japan;

^bNational Astronomical Observatory of Japan, National Institutes of Natural Sciences, 2-21-1 Osawa, Mitaka, Tokyo 181-8588, Japan;

^cAstro Research Corporation, 134 Godo, Hodogaya, Yokohama 240-0005, Japan;

^dMeisei Electric Co., Ltd., 3-24-1 Yurigaoka, Moriya, Ibaragi 302-0192, Japan;

^eSmithsonian Astrophysical Observatory, 60 Garden Street, Cambridge, MA 02138, U.S.A.;

^fNASA Marshall Space Flight Center, 320 Sparkman Drive, Huntsville, AL 35805, U.S.A

ABSTRACT

We present scientific as well as engineering overview of the X-Ray Telescope (XRT) aboard the Japanese *Solar-B* mission to be launched in 2006, with emphasis on the focal plane CCD camera that employs a 2k×2k back-thinned CCD. Characterization activities for the flight CCD camera made at the National Astronomical Observatory of Japan (NAOJ) are discussed in detail with some of the results presented.

Keywords: Sun, X-rays, CCD, X-ray Telescope

1. INTRODUCTION

The outer atmosphere of the Sun, the solar corona, is most clearly discernible when seen in soft X-rays. Since the early rocket experiments in late 1960's, it has become widely recognized that soft X-ray imagery of the Sun provides powerful means to investigate physical conditions of hot plasmas (whose temperature as high as 1 MK, or even more) that prevails in the corona. As the high-temperature plasmas in the corona are forced to move along coronal magnetic field, soft X-rays from the Sun, emitted by such plasmas, reflects magnetic field structure of the corona. Imaging observations of the solar corona with the Soft X-ray Telescope (SXT)¹ aboard the *Yohkoh* satellite² have revealed that the corona is far more dynamic than ever been thought; coronal structures, *i.e.*, magnetic field configuration in the corona, frequently showing dynamic evolution in a wide range of time scales (from less than a minute to days) as well as spatial scales. It is noteworthy that observations with *Yohkoh* have also clarified that such dynamic evolution of the corona, followed by energy release, in the form of plasma heating and particle acceleration, is associated with magnetic reconnection that takes place in the corona^{3,4}.

*sakao@solar.isas.jaxa.jp; phone +81-42-759-8210; fax +81-42-759-8526

Based on the findings made by *Yohkoh*, the next Japanese solar mission *Solar-B* (Fig. 1), which is to be launched by the Institute of Space and Astronautical Science, Japan Aerospace Exploration Agency (ISAS/JAXA) in 2006, aims to investigate photosphere-corona connection, in other words, relationship between magnetic activities on the photosphere and their coronal consequences such as transport, storage, and dissipation of magnetic energy in the corona^{5,6}. The *Solar-B* observatory consists of three telescopes, Solar Optical Telescope (SOT), X-Ray Telescope (XRT)⁷, and EUV Imaging Spectrometer (EIS). The SOT employs a 50 cm-diameter primary mirror and will carry out quantitative vector magnetic field observations with its spatial resolution as high as 0.02". The EIS performs detailed temperature and velocity diagnostics on coronal as well as transient region plasmas, attempting to detect plasma flows associated with magnetic reconnection.

The XRT is a successor of the SXT aboard *Yohkoh*. It also employs a grazing incidence optics, but with improved spatial resolution (consistent with 1" CCD pixel size which should be compared with ~2.5" in the case of SXT) while maintaining similar exposure cadence as SXT. Furthermore it should be stressed that, by use of a back-thinned CCD coupled with an optimized set of focal plane thin-metal filters, the XRT is capable of imaging soft X-ray sources in the wavelength range beyond 60 Å in addition to those below it. This is a major difference from *Yohkoh* SXT in that the XRT can observe not only high-temperature plasmas (> 2 MK) seen with SXT, but also low-temperature (< 2 MK, reaching even below 1 MK) plasmas which comprise a significant amount of coronal plasmas. With such enhanced temperature range for observing coronal plasmas, coupled with increased high spatial resolution, the XRT will be able to perform detailed imaging observations on a wide variety of coronal plasmas in a temperature range continuously covering from below 1 MK to above 30 MK (superhot plasmas generated during the course of flares) and to make temperature maps for such plasmas. Thus the XRT is expected to observe various coronal activities in association with magnetic activities on the photosphere (observed with SOT) and to investigate coronal consequences of the magnetic activities (transport, storage, and dissipation of magnetic energy) together with EIS.

The XRT is a joint US-Japan project with Smithsonian Astrophysical Observatory (SAO) and NASA developing the optics and the mechanisms while the focal plane CCD camera being developed by the National Astronomical Observatory of Japan (NAOJ) and ISAS/JAXA. In Section 2, we give brief overview of the telescope as well as the camera. In Section 3, a detailed description on the calibration activities on the camera is given followed by concluding remarks in Section 4.



Fig. 1. The Solar-B satellite.

2. BRIEF OVERVIEW OF THE TELESCOPE

2.1. The telescope

The XRT, whose length ~3 m, consists of an optimized Wolter-I-like grazing incidence soft X-ray optics together with a co-focal visible light optics. A schematic drawing of the entire telescope is given in Fig. 2. Both soft X-ray and visible

light images are focused on a single CCD located in the CCD camera described below. The X-ray/visible light selection is done by inserting either a thin-metal or a glass filter mounted on filter wheels into the light path. There is also a shutter (visible-light shutter; VLS) in front of the visible light lens at the top of the telescope which is opened only when taking visible light images. A pre-filter is mounted at the entrance aperture for the X-ray mirror.

At the rear end of the telescope tube in front of the focal plane CCD camera is attached an assembly of (1) a focal plane shutter, (2) two filter wheels for mounting thin-metal filters and a glass filter, and (3) focus mechanism motor. Combination of images taken with different filters on the filter wheels (each of the wheels has six mounting positions for filters) will enable us to obtain temperature maps of observing targets in the field-of-view of the XRT. Fig. 3 shows temperature response of the metal filters with X-ray transmittance of the pre-filter, effective area of the X-ray mirror, and the measured quantum efficiency of the CCD detector⁸ taken into account. The telescope tube is made of CFRP which sustains both the front assembly (the X-ray mirror and the visible light lens) and the rear assembly.

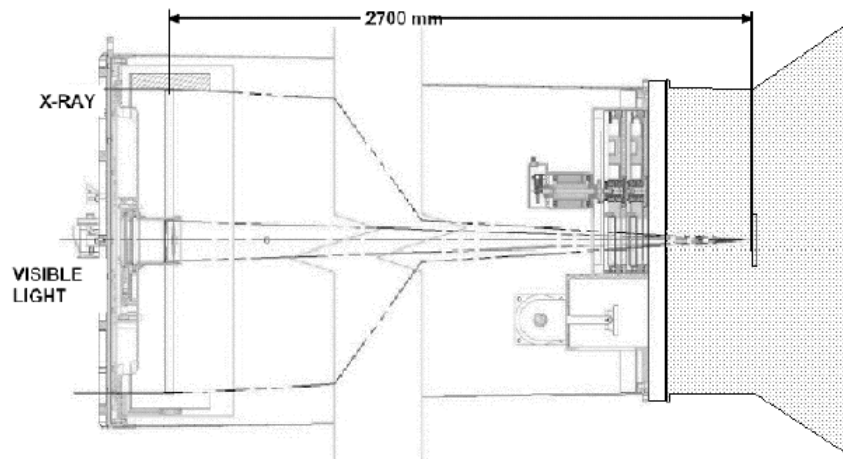


Fig. 2. A schematic drawing of the X-Ray Telescope (XRT). The left hand side indicates front assembly of the telescope (a grazing incidence X-ray mirror and a visible light lens), while in the right hand side, rear assembly (a focal plane shutter, filter wheels, and a focus motor) and the CCD camera portion (shown in gray) are shown.

Table 1. Basic features of the XRT.

X-Ray Optics	
Optics	Optimized Wolter-I-like grazing incidence optics
Focal length	2708 mm
Mirror micro-roughness	6 Å expected (mirror under polish)
Aperture size	> 340 mm
Spatial resolution	68% of encircled energy in 2 arcsec (at 0.523 keV)
Wavelength range	2–200 Å
Effective area	> 1.0 cm ² at 0.523 keV
Visible Light Optics	
Focal length	2708 mm
Wavelength	4305 Å (G-band)
Focal Plane CCD Camera	
CCD device	E2V (former Marconi) 2048×2048 back-illuminated (13.5 μm pixel size)
Field of view	34×34 arcmin (capable of covering the whole Sun)
Image readout	500 kpixel/s

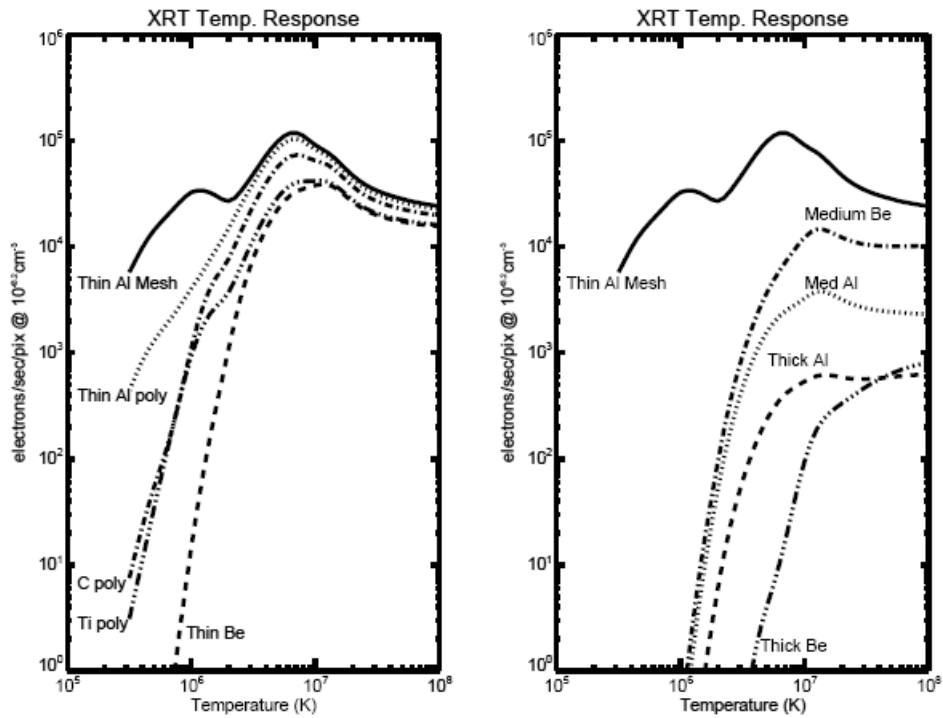


Fig. 3. Temperature response of the XRT.

2.2. The CCD camera

At the rear end of the telescope tube the CCD camera, developed by the Japanese XRT team, is mounted (Fig. 4). The camera contains a back-thinned $2k \times 2k$ CCD device ($13.5 \mu\text{m}$ pixel size) delivered by E2V (formerly Marconi Applied Technologies). In order to suppress generation of dark current during long-exposure observations, the CCD will be cooled down on orbit by passive cooling down to below -70 degC (below $\sim -43 \text{ degC}$ even in the hot-worst operating condition with a non-eclipsing orbit). Besides cooling the CCD, the camera employs a CCD bakeout (de-contamination) heater with which, according to a recent telescope-level thermal balance testing, the CCD is expected to be warmed up above $+30 \text{ degC}$ while its surroundings (including the rear assembly of the telescope tube) at around, or below, $+20 \text{ degC}$ even in the cold-worst operating condition. The camera chassis is made of Titanium alloy (Ti-6Al-4V) to maintain positional accuracy of the CCD against on-orbit temperature variations.

A unique feature of the CCD camera is that it is equipped with a mechanism which allows the CCD to move, by commands sent from the ground, along the optics axis by $\pm 1 \text{ mm}$ while maintaining the above thermal performance. The mechanism will provide not only post-launch focus adjustment capability, but it also provides us, by adjusting the CCD position along the optics axis, with flexible sets of field-of-view versus angular resolution combinations for focal plane images depending on observing targets. With this focus adjustment capability, the XRT will be able to, for example, observe a region well covering the field-of-view of both SOT and EIS with the angular resolution of RMS blurr diameter being less than 1 arcsec , or to observe nearly the entire solar disk with the blurr diameter of less than $\sim 2\text{-}2.5 \text{ arcsec}$, as shown in Fig. 5.

The CCD camera is controlled by a camera electronics. It consists of a pre-amplifier unit inside the camera and a separate electronics box. The electronics box applies CCD drive clocks and bias voltages to the camera and receives CCD analog video output signals. The video signals are A-to-D converted into 14 bits inside the electronics box while the upper 12 bits are transferred to the spacecraft Mission Data Processor (MDP) for telemetry data. The CCD device has

two readout ports (R-port and L-port) with the R-port used as default while the L-port is for backup. Selection of the two ports is to be done by a command from the ground.

Special care was taken to suppress CCD noise as much as available, which led us to take optimized ground configuration for the camera. The CCD package, together with its housing, is grounded to the (clean) electronic signal ground and is isolated from the chassis ground. The signal ground and the chassis ground are connected as a single-point ground connection outside the XRT. Also, yet another electronic ground was introduced to serve as ground for CCD clocks to avoid, as much as possible, effect of clocking spikes into the clean signal ground. (The clock ground and the signal ground are connected as a single-point ground inside the electronics box.) In order to accommodate to such ground configuration, electrical isolation structure is also implemented inside the camera.

Sequence of CCD images are taken by exposure commands with exposure parameters (such as exposure duration, filters to be inserted in the light path, region on the CCD to be read out, on-chip CCD pixel binning, and so forth) sent to the XRT from MDP. During observation, the MDP sends out these exposure commands/parameters based on observation tables inside MDP which enables to achieve flexible observations depending on a wide variety of observing targets. Also, the XRT observation will be conducted based on autonomous image processing capability of MDP, e.g., by automatic exposure control (AEC), automatic region selection (ARS), and automatic flare detection (FLD). Description of XRT observations with MDP is given elsewhere⁹.

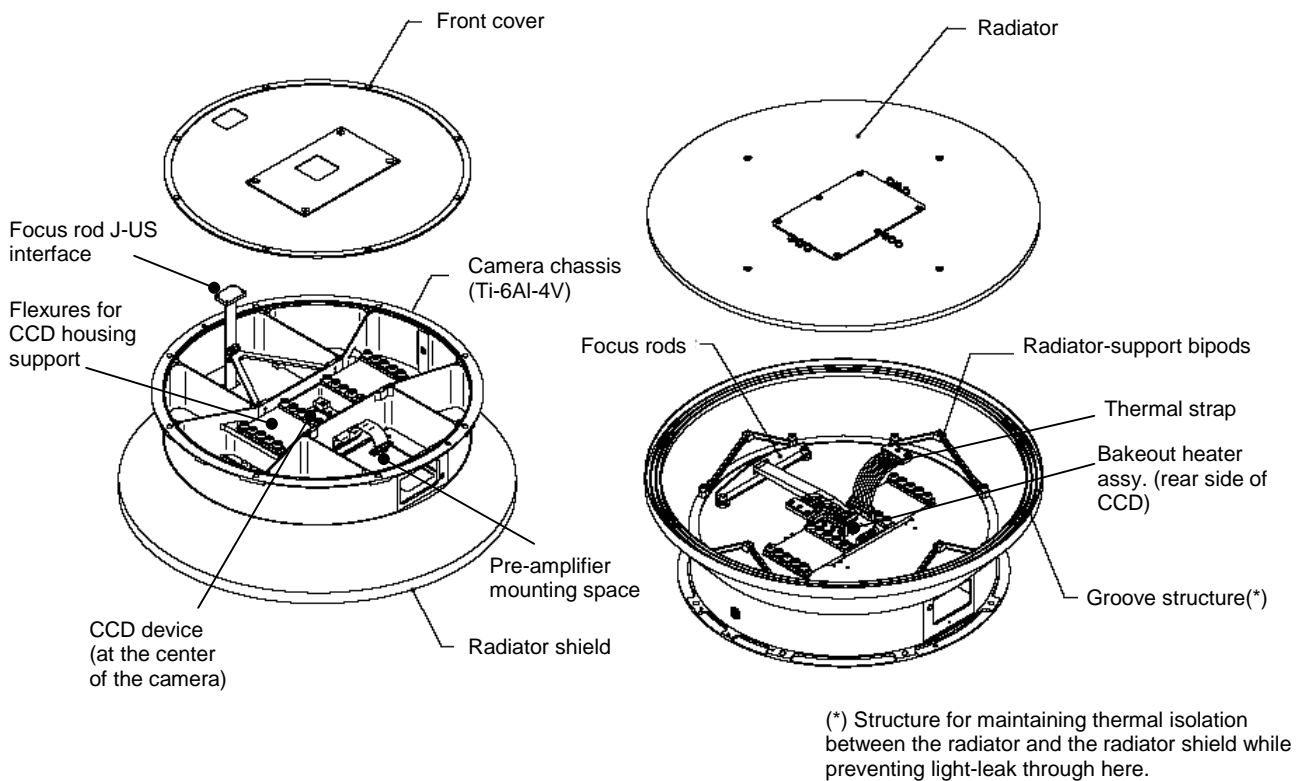


Fig. 4. Schematic drawing of the CCD camera. *Left*: Seen from the telescope side (Sun-facing direction), with the front cover detached. *Right*: From the rear side (radiator side), with the radiator detached.

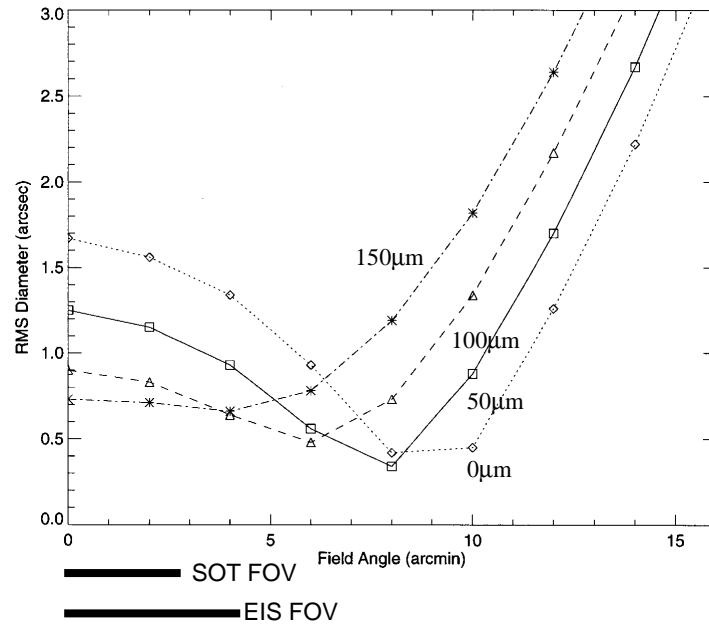


Fig. 5. Focal plane profile of the XRT; RMS blur diameter against off-axis field angle at various CCD locations along the optics axis (shown as 0, 50, 100, and 150 μm in the figure). Field-of-view sizes of SOT and EIS are also shown.

3. CCD CAMERA CHARACTERIZATION

An extensive characterization activity on the flight CCD camera¹⁰ was conducted by a team led by H. Hara of NAOJ in the year 2003, prior to the delivery of the camera to SAO. The characterization activity includes: (1) System gain calibration of the camera with an ^{55}Fe isotope, (2) dark current characterization, (3) charge transfer efficiency (both for parallel and serial transfers), (4) output linearity check, (5) quantum efficiency measurements in X-ray and EUV wavelengths, (6) flatness in CCD sensitivity, and (7) check for conservation of electrons with on-chip multiple pixel binnings. All these activities were performed under Class 100 clean room environment (measured class ~ 0) prepared at NAOJ. Characterization items (1), (4), and (5) were performed during a dedicated measurement time frame (in May 2003) while measurements for items (2), (3), and some portion of (1) were carried out as part of measurements during the camera thermal cycle test (late May 2003). Other items, including some portion of (4), were performed by making use of appropriate time frames during, *e.g.*, running test for the camera electronics.

For the characterization activity, the CCD camera was mounted inside a vacuum chamber in the NAOJ clean room (Fig. 6). The internal environment of the chamber was monitored by a TQCM to make sure there is no contamination source in the chamber that otherwise would degrade CCD sensitivity. Also, as the length between the CCD electronics box and the CCD camera (pre-amplifier) needs to be kept less than, say, 30 cm so as to maintain good CCD noise quality, the electronics box had to be located inside the chamber as well. For this purpose, an airtight box was developed into which the electronics box was installed with atmospheric pressure environment. By use of the airtight box located inside the chamber, we could safely prevent outgas of the electronics box from spreading out to the chamber environment. Note when assembled to the spacecraft, the electronics box is mounted inside the bus module of the satellite which is not seen from the XRT by a bus panel. A cold finger, attached to non-flight radiators, was also developed to cool down the CCD with liquid nitrogen during the measurements.

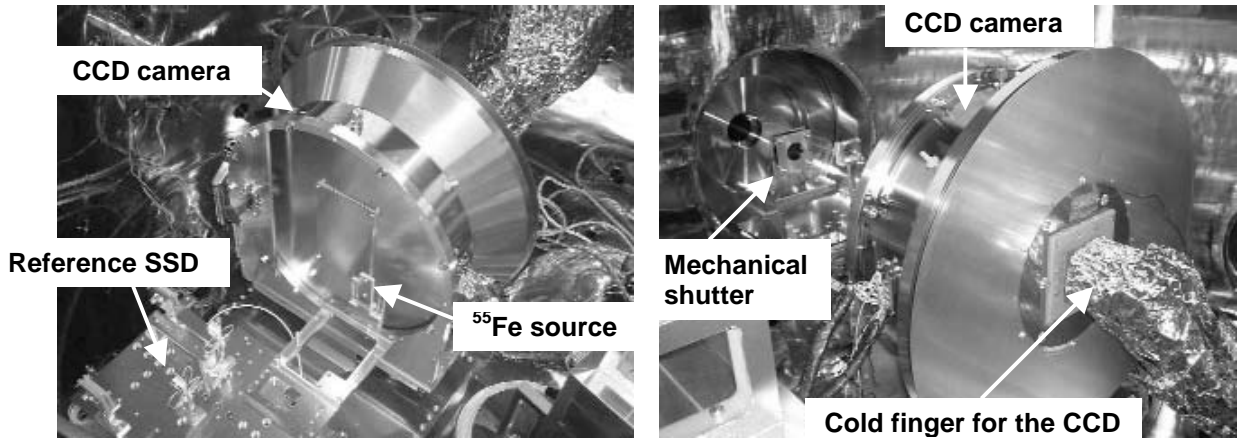


Fig. 6. Measurement setup for the X-ray/EUV characterization tests.

Some representative measurements are described below, while a set of characterization results summarized in Table 2.

3.1. Camera system gain measurement

The measurement was carried out with an ^{55}Fe isotope. A histogram in thin lines in each panel of Fig. 7 shows number of events (pixels) obtained by subtraction of an image from other one, both containing ^{55}Fe events, for the R-port readout at various temperatures. Subtraction is for eliminating contribution of dark spikes in the images. The peak at around 110 ADU (in 14 bits) seen in each panel corresponds to events by ^{55}Fe . (Note the data reduction described here also produces another peak at around -110 ADU which is not shown in the figure.) In each of the ^{55}Fe event peaks, we notice $\text{Mk K}\alpha$ and $\text{Mn K}\beta$ features (the latter is discernible at ~ 120 ADU), but at the same time, a tail feature elongating towards lower-ADU direction caused by the so-called “split events”. In order to properly treat contribution from such split events, 3×3 pixel summations were performed for each of the single ^{55}Fe event the result of which is shown in thick histograms in the figure. The system gain of the camera, for each of the R- and L-port readout, is thus derived by taking into account that a single ^{55}Fe event generates 1614 electrons. The result is summarized in Table 2.

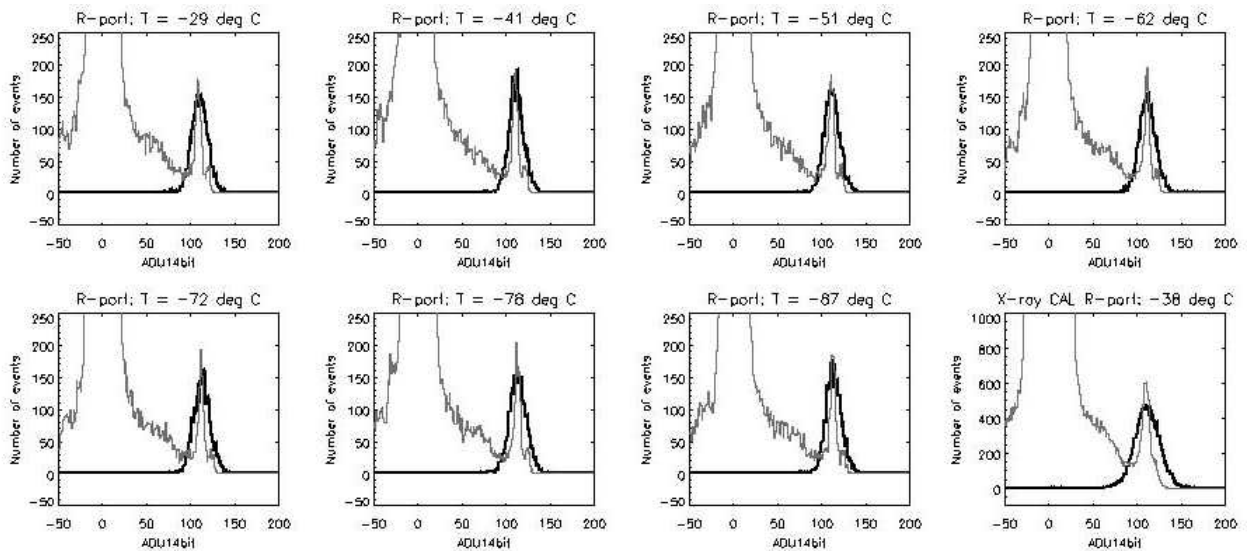


Fig. 7. Histograms for ^{55}Fe events with R-port readout at various CCD temperatures (thin line), overlaid with those with the split-event effect corrected (thick line). See text for details.

3.2. Dark current characterization

A set of three dark frame exposures, 2 ms, 4 s, and 64 s was used for the dark current characterization of the camera at each different CCD temperatures. Fig. 8(a) shows a sample dark frame image obtained by subtracting a 4-s exposure image from a 64-s exposure image thus eliminating contribution of dark current generation during parallel charge transfer. Measurements of the dark current at various temperatures (averaged over the CCD imaging area) are summarized in Fig. 8(b), yielding dark current figure of merit¹¹ of 0.4 nA/cm². The camera system gain, described in Section 3.1, is used here for converting from ADU to electrons. The apparent deviation from the dotted curve below -75 degC in the figure is caused by too-low dark current counts with 1×1 pixel data; more accurate estimate of dark current rate with multiple pixel binning data (such as 2×2 on-chip summation) is under progress by making use of a telescope-level thermal balance test.

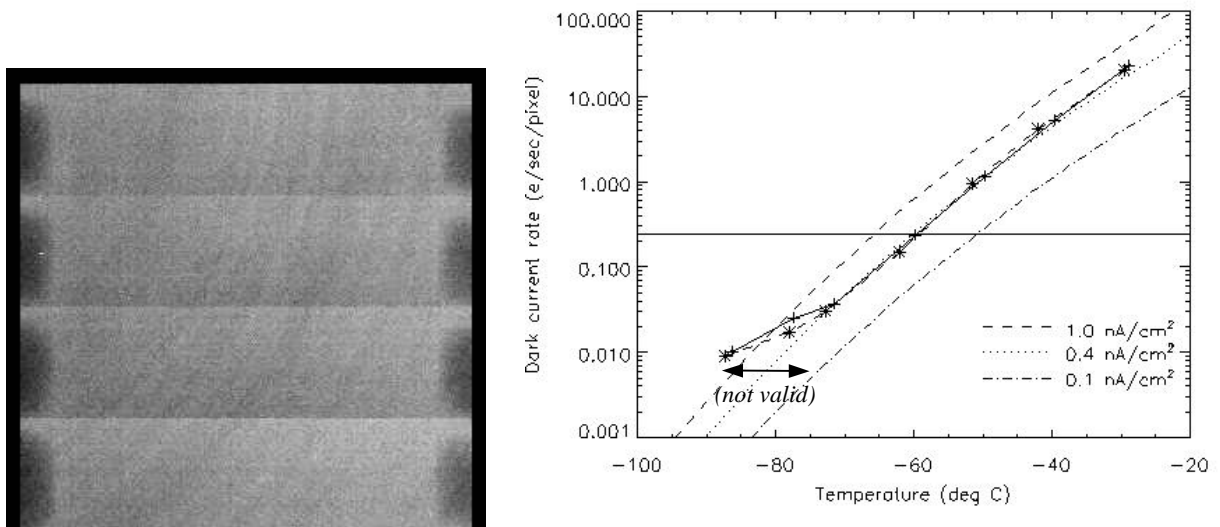


Fig. 8. *Left:* (a) A sample dark frame image with 60-s accumulation; a 4-s dark frame image subtracted from that of 64-s. *Right:* (b) CCD dark current rate as a function of temperature. The horizontal line indicates a reference level of 1 [14bitADU/60s]. Note the deviation from the dotted line below -75 degC (shown by an arrow in the figure) is caused by too-low dark current counts with 1×1 pixel data.

3.3. Quantum efficiency measurement

The X-ray/EUV quantum efficiency (QE) measurement on the CCD camera was performed with an X-ray monochromator which is a grazing-incidence In-Focus Monochromator SXR-0.5 made by Hettrick Scientific with Manson model 2 Ultra-soft X-ray source made by Austin Instruments Inc., and an EUV monochromator, a grazing-incidence monochromator of Jovin-Yvon with a Penning discharge source. A reference solid-state detector (SSD), AXUV-100G provided by the International Radiation Detectors, Inc. (IRD), was located in between the X-ray/EUV light source and the CCD camera. The SSD, connected to a Keithley 617 Digital Electrometer for current measurement, was mounted on a movable stage so that either the reference SSD or the CCD itself can have X-ray/EUV light illumination. A mechanical shutter was placed in front of the CCD camera (see Fig. 6 for the configuration).

Results from the QE measurements are summarized in Fig. 9. The top panel shows ratio of the two QE sets between the CCD and the SSD. The bottom panel indicates QE of the CCD in the X-to-EUV wavelengths, with that of the SSD (partly estimated) taken into account. An absolute measurement on the SSD QE is being planned. The solid curve in the bottom panel of Fig. 9 is based on a QE model described in a literature¹².

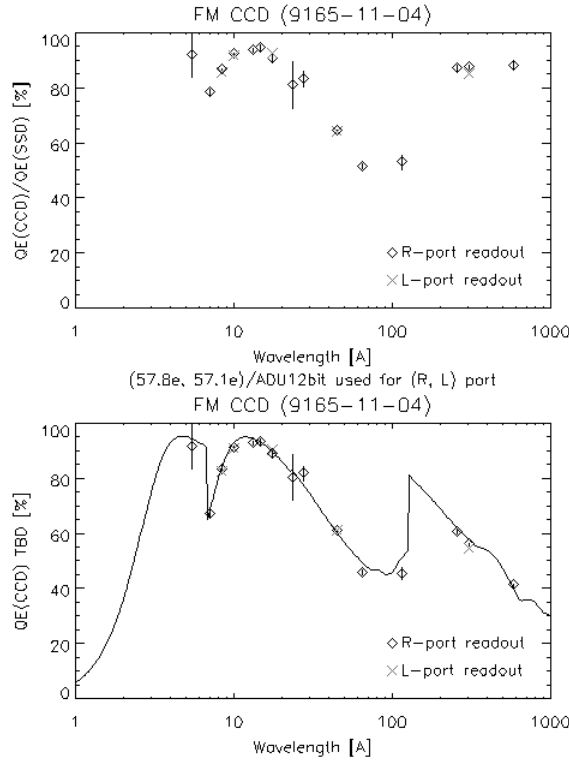


Fig. 9. *Top*: Ratio of QE between the flight CCD and the SSD. *Bottom*: QE of the CCD with a model curve. See text for details.

Table 2. Summary of the CCD camera characterization measurements (preliminary).

Item	Description
CCD camera gain	R-port: $59.1 + 0.026 T (K) [e^-/12\text{bitADU}]$ L-port: $58.8 + 0.034 T (K) [e^-/12\text{bitADU}]$
Dark current figure of merit	$0.4 [\text{nA}/\text{cm}^2]$
Charge transfer efficiency (CTE)	Parallel transfer: > 0.999996 Serial transfer: $> 0.999999 (-93 \text{ degC} < T < -50 \text{ degC})$
Output linearity	Deviation less than 2 % up to 3000 DN (12bitADU)
Full well capacity	$2.0 \times 10^5 [e^-]$
Quantum efficiency (QE) ^(*)	0.93 @ 13A, 0.61 @ 45A, 0.46 @ 114A, 0.56 @ 304A
Flatness in CCD sensitivity	Deviation less than 5%.

^(*) Tentative; absolute measurement on the QE of the reference SSD used in the calibration to be performed.

4. CONCLUDING REMARKS

As described in Section 3, extensive characterization effort has so far been made on the CCD camera of the XRT, leaving only a small amount of issues to be performed (such as calibration of the reference SSD for precise determination of the CCD QE, and dark current characterization below -75 degC). Such well-characterized CCD camera, in combination with the advanced and unique capability of the telescope mentioned in Section 2, will enable us to perform, in detail, quantitative investigation on the physical condition of coronal plasmas. The flight CCD camera was delivered to SAO in August 2003 and has been mated to the telescope structure. The entire XRT will be delivered to

ISAS/JAXA for a spacecraft-level test soon. We expect that the XRT, in combination with SOT and EIS aboard *Solar-B*, will lead us to new discoveries on coronal activities and to reveal fundamental mechanisms behind them.

ACKNOWLEDGEMENTS

The authors are grateful to the staff of Advanced Technology Center (ATC) at NAOJ for their continuous support during the course of the CCD camera experiments, particularly to Mr. T. Nishino and his colleagues at the ATC machine shop for their valuable and timely help in developing experiment-supporting tools. Messrs. M. Noguchi and M. Miyashita of NAOJ are also deeply acknowledged for their help in preparation/setup for the experiments.

REFERENCES

1. Tsuneta, S., Acton, L., Bruner, M., Lemen, J., Brown, W., Carvalho, R., Catura, R., Freeland, S., Jurcevic, B., Morrison, M., Ogawara, Y., Hirayama, T., and Owens, J., “The Soft X-ray Telescope for the Solar-A Mission”, *Solar Phys.*, **136**, pp. 37–67, 1991.
2. Ogawara, Y., Takano, T., Kato, T., Kosugi, T., Tsuneta, S., Watanabe, T., Kondo, I., and Uchida, Y., “The Solar-A Mission: An Overview”, *Solar Phys.*, **136**, pp. 1–16, 1991.
3. Masuda, S., Kosugi, T., Hara, H., Tsuneta, S., and Ogawara, Y., “A loop-top hard X-ray source in a compact solar flare as evidence for magnetic reconnection”, *Nature*, **371**, pp. 495–497, 1994.
4. Tsuneta, S., “Structure and Dynamics of Magnetic Reconnection in a Solar Flare”, *Astrophys. J.*, **456**, pp. 840–849, 1996.
5. Kubo, M., Shimizu, T., and Lites, B.W., “The Evolution of Vector Magnetic Fields in an Emerging Flux Region”, *Astrophys. J.*, **595**, pp. 465–482, 2003.
6. Katsukawa, Y., Ph.D. Thesis, The University of Tokyo, 2004.
7. Golub, L., DeLuca, E.E., Bookbinder, J.A., Cheimets, P., Shibasaki, K., Sakao, T., and Kano, R., “High-resolution grazing incidence telescope for the Solar-B observatory”, *Proc. SPIE*, **4139**, pp. 313–327, 2000.
8. Hara, H., et al., in preparation.
9. Kano, R., Hara, H., Shimojo, M., Tsuneta, S., Sakao, T., Matsuzaki, K., Kosugi, T., Golub, L., DeLuca, E., Bookbinder, J., Cheimets, P., Owens, J., and Hill, L., “Characteristics of Solar-B X-ray Telescope (XRT)”, in *Proc. Fifth Solar-B Science Meeting, The Solar-B Mission and the Forefront of Solar Physics*, ASP Conference Series, in press.
10. Hara, H., “FM XRT-S Calibration Report (Preliminary)”, in *SOLAR-B Soft X-ray Telescope (XRT) Flight CCD Camera System (XRT-S, XRT-E) Data Package (Preliminary version)*, Solar-B XRT Team, pp. 48–88, 2003.
11. Janesick, J.R., “Scientific Charge-Coupled Devices”, SPIE Press, 2001.
12. Stern, R.A., Shing, L., and Blouke, M.M., “Quantum efficiency measurements and modeling of ion-implanted, laser annealed charge-coupled devices: x-ray, extreme ultraviolet, ultraviolet, and optical data”, *Applied Optics*, **33**, pp. 2521–2533, 1994.